

Probing shell structure and shape changes in neutron-rich sulfur isotopes through transient-field g -factor measurements on fast radioactive beams of ^{38}S and ^{40}S .

A.D. Davies,^{1,2} A.E. Stuchbery,³ P.F. Mantica,^{1,4} P.M. Davidson,³
A.N. Wilson,^{3,5} A. Becerril,^{1,2} B.A. Brown,^{1,2} C.M. Campbell,^{1,2}
J.M. Cook,^{1,2} D.C. Dinca,^{1,2} A. Gade,¹ S.N. Liddick,^{1,4} T.J. Mertzimekis,¹
W.F. Mueller,¹ J.R. Terry,^{1,2} B.E. Tomlin,^{1,4} K. Yoneda,¹ and H. Zwahlen^{1,2}

¹*National Superconducting Cyclotron Laboratory,
Michigan State University, East Lansing, MI 48824 USA*

²*Department of Physics and Astronomy,
Michigan State University, East Lansing, MI 48824 USA*

³*Department of Nuclear Physics, The Australian
National University, Canberra, ACT 0200, Australia*

⁴*Department of Chemistry, Michigan State University, East Lansing, MI 48824 USA*

⁵*Department of Physics, The Australian National
University, Canberra, ACT 0200, Australia*

(Dated: September 24, 2018)

Abstract

The shell structure underlying shape changes in neutron-rich nuclei near $N = 28$ has been investigated by a novel application of the transient field technique to measure the first-excited state g factors in ^{38}S and ^{40}S produced as fast radioactive beams. There is a fine balance between proton and neutron contributions to the magnetic moments in both nuclei. The g factor of deformed ^{40}S does not resemble that of a conventional collective nucleus because spin contributions are more important than usual.

PACS numbers: 21.10.Ky,21.60.Cs,27.30.+t,27.40.+z,25.70.De

The fundamental question of how major shell closures, or magic numbers, change in neutron-rich nuclei remains unresolved. At present there is conflicting evidence concerning the $N = 28$ shell gap in nuclei approaching the neutron dripline. From the measured β -decay half-life it has been suggested that ${}^{42}_{14}\text{Si}_{28}$ is strongly deformed, implying a quenching of the $N = 28$ gap [1], whereas knockout reactions on ${}^{42}\text{Si}$ give evidence for a nearly spherical shape [2]. Low-excitation level structures and $B(E2)$ values imply that the nearby even sulfur isotopes between $N = 20$ and $N = 28$ undergo a transition from spherical at ${}^{36}_{16}\text{S}_{20}$, to prolate deformed in ${}^{40}_{16}\text{S}_{24}$ and ${}^{42}_{16}\text{S}_{26}$, and that the $N = 28$ nucleus ${}^{44}_{16}\text{S}_{28}$ appears to exhibit collectivity of a vibrational character [3, 4, 5, 6]. However the evolution of deformation in these nuclei has underlying causes that remain unclear. Some have argued that a weakening of the $N = 28$ shell gap is important [6], while others have argued that the effect of adding *neutrons* to the $f_{7/2}$ orbit is primarily to reduce the *proton* $s_{1/2}$ - $d_{3/2}$ gap and that a weakening of the $N = 28$ shell gap is not needed to explain the observed collectivity near ${}^{44}\text{S}$ [7]. There have been several theoretical studies discussing the erosion of the $N = 28$ shell closure and the onset of deformation (e.g. Refs. [8, 9] and references therein).

To resolve questions on the nature and origins of deformation near $N = 28$, we have used a novel technique to measure the g factors of the 2^+_1 states in ${}^{38}_{16}\text{S}_{22}$ and ${}^{40}_{16}\text{S}_{24}$. The g factor, or gyromagnetic ratio, is the magnetic moment divided by the angular momentum. The existence of deformation in nuclei has long been associated with strong interactions between a significant number of valence protons and neutrons, particularly in nuclei near the middle of a major shell. Without exception the deformed nuclei studied to date have g factors near the hydrodynamical limit, Z/A , reflecting the strong coupling between protons and neutrons, and a magnetic moment dominated by the orbital motion of the proton charge with small contributions from the intrinsic magnetic moments of either the protons or the neutrons. In transitional regions g factors have considerable sensitivity to the proton and/or neutron contributions to the state wavefunctions, particularly if the intrinsic spin moments of the nucleons come to the fore.

The present Letter presents the first application of a high-velocity transient-field (HVTF) technique [10] to measure the g factors of excited states of fast radioactive beams. In brief, intermediate-energy Coulomb excitation [11] is used to excite and align the nuclear states of interest. The nucleus is then subjected to the transient field in a higher velocity regime than has been used previously for moment measurements, which causes the nuclear spin

to precess. Finally, the nuclear precession angle, to which the g factor is proportional, is observed via the perturbed γ -ray angular correlation measured using a multi-detector array. It is important to note that the transient-field technique has sensitivity to the *sign* of the g factor, which in itself can be a distinguishing characteristic of the proton/neutron contributions to the state under study, since the signs of the spin contributions to the proton and the neutron g factors are opposite.

The transient field (TF) is a velocity-dependent magnetic hyperfine interaction experienced by the nucleus of a swift ion as it traverses a magnetized ferromagnetic material [12, 13]. For light ions ($Z \leq 16$) traversing iron and gadolinium hosts at high velocity, the dependence of the TF strength on the ion velocity, v , and atomic number, Z , can be parametrized [10, 14] as

$$B_{\text{tf}}(v, Z) = AZ^P(v/Zv_0)^2 e^{-\frac{1}{2}(v/Zv_0)^4}, \quad (1)$$

where $v_0 = c/137$ is the Bohr velocity. A fit to data for iron hosts yielded $A = 1.82(5)$ T with $P = 3$ [10]. The maximum TF strength is reached when the ion velocity matches the K -shell electron velocity, $v = Zv_0$. Since the transient field arises from polarized electrons carried by the moving ion its strength falls off as the ion velocity exceeds Zv_0 and becomes fully stripped; a transient-field interaction will not occur for fast radioactive beams with energies near 100 MeV/nucleon until most of that energy is removed.

The experiment was conducted at the Coupled Cyclotron Facility of the National Superconducting Cyclotron Laboratory at Michigan State University. Secondary beams of ^{38}S and ^{40}S were produced from 140 MeV/nucleon primary beams directed onto a ~ 1 g/cm 2 ^9Be fragmentation target at the entrance of the A1900 fragment separator [15]. An acrylic wedge degrader 971 mg/cm 2 thick and a 0.5% momentum slit at the dispersive image of the A1900 were employed. The wedge degrader allowed the production of highly pure beams and also reduced the secondary beam energy to ~ 40 MeV/nucleon. Further details of the radioactive beams are given in Table I. The ^{38}S (^{40}S) measurement ran for 81 (68) hours.

Figure 1 shows the experimental arrangement. The radioactive beams were delivered onto a target which consisted of a 355 mg/cm 2 Au layer backed by a 110 mg/cm 2 Fe layer of dimensions 30×30 mm 2 . The target was held between the pole tips of a compact electromagnet that provided a magnetic field of 0.11 T, sufficient to fully magnetize the Fe layer. To minimize possible systematic errors, the external magnetic field was automatically

TABLE I: Production and properties of radioactive beams.

Primary beam		Secondary beam			
Ion	Intensity (pnA)	Ion	E (MeV)	Intensity (pps)	Purity (%)
^{40}Ar	25	^{38}S	1547.5	$2 \cdot 10^5$	> 99
^{48}Ca	15	^{40}S	1582.5	$2 \cdot 10^4$	> 95

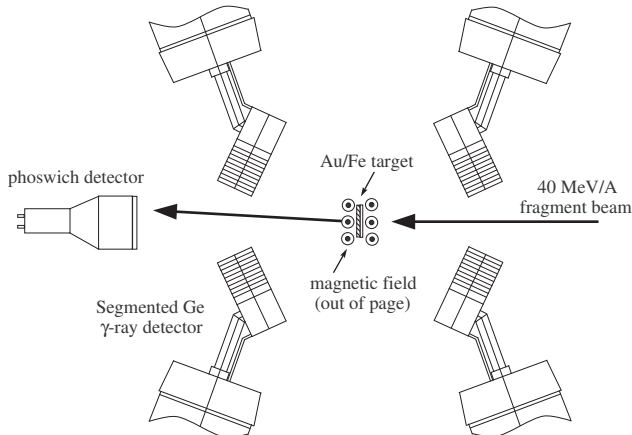


FIG. 1: Schematic view of the experimental arrangement from above. Only the four SeGA detectors perpendicular to the magnetic field axis are shown. There are ten other SeGA detectors (see text) which are not shown for clarity.

reversed every 600 s.

Table II summarizes the properties of the 2_1^+ states, the key aspects of the energy loss of the sulfur beams in the target, the precession results and the extracted g factors. The high- Z Au target layer serves to enhance the Coulomb excitation yield and slow the projectiles to under 800 MeV, while the thick iron layer results in a long interaction time with the transient field, maximizing the spin precession. The sulfur fragments emerge with energies in the range from ~ 80 MeV to ~ 200 MeV. Most of this energy spread stems from the energy width of the radioactive beam.

Projectiles scattering forward out of the target were detected with a 15.24 cm diameter plastic scintillator phoswich detector placed 79.2 cm downstream of the target position. The maximum scattering angle of 5.5° limits the distance of closest approach to near the nuclear

interaction radius in both the Au and Fe target layers. Positioning the particle detector downstream also lowers the exposure of the γ -ray detectors to the radioactive decay of the projectiles.

To detect de-excitation γ rays, the target chamber was surrounded by 14 HPGe detectors of the Segmented Germanium Array (SeGA) [16]. The SeGA detectors were positioned with the crystal centers 24.5 cm from the target position. Six pairs of detectors were fixed at symmetric angles $(\pm\theta, \phi) = (29^\circ, 90^\circ), (40^\circ, 131^\circ), (60^\circ, 61^\circ), (139^\circ, 46^\circ), (147^\circ, 143^\circ),$ and $(151^\circ, 90^\circ)$, where θ is the polar angle with respect to the beam axis and ϕ is the azimuthal angle measured from the vertical direction, which coincides with the magnetic field axis. Each $\pm\theta$ pair is in a plane that passes through the center of the target; $(-\theta, \phi) = (\theta, \phi+180^\circ)$. Two more detectors were placed at $\theta = 90^\circ$ and $\theta = 24^\circ$. All 14 detectors were used to measure the γ -ray angular correlations concurrently with the precessions. Since the precession angles are small, the unperturbed angular correlation can be reconstructed by adding the data for the two directions of the applied magnetic field.

Coincidences between the phoswich particle detector and SeGA were recorded, and γ -ray spectra gated on sulfur recoils and corrected for random coincidences were produced. Doppler-corrected spectra were also produced using the angular information from the SeGA detector segments and the particle energy information from the phoswich detector on an event-by-event basis, which is essential because of the spread in particle velocities. Figure 2 shows examples of the γ -ray spectra. From the measured Doppler shift of the deexcitation γ rays in the laboratory frame, the average after-target ion velocities were determined. The velocity distribution of the exiting ^{40}S ions was also measured by shifting the phoswich detector by ± 15 cm from its normal position and observing the change in the flight times of the projectiles. These procedures firmly establish that the sulfur ions were slowed through the peak of the TF strength at Zv_0 into the region where it has been well characterized [10, 13].

The 2^+ peak areas averaged 925 counts/detector per field direction for ^{38}S and 400 counts/detector per field direction for ^{40}S , in each of the six angle pairs of SeGA detectors used for extracting the precessions.

The angular correlation of γ rays was calculated with the program GKINT [17] using the theory of Coulomb excitation [18]. Recoil-in-vacuum effects were evaluated based on measured charge-state fractions for sulfur ions emerging from iron foils [19]. Good agreement

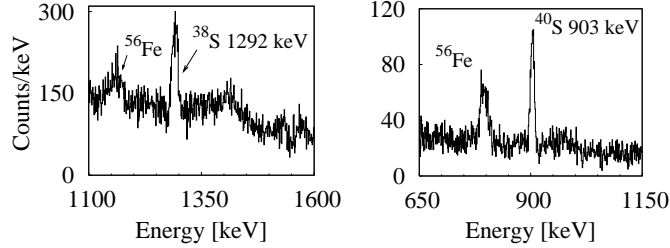


FIG. 2: Doppler-corrected γ -ray spectra at $\theta = 40^\circ$ for ^{38}S (left) and ^{40}S (right). The sulfur and iron peaks are labeled. The broad feature to the right of the 1292 keV line is mainly its Doppler tail, due to decays within the target.

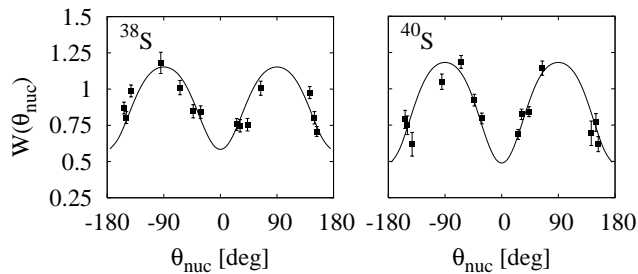


FIG. 3: Angular correlations for ^{38}S and ^{40}S in the frame of the projectile nucleus. Data are normalized to the calculated angular correlation. The difference in anisotropy stems from the alignment produced by Coulomb excitation, which depends on the ratio of $E(2^+)$ to the beam velocity.

was found between the calculated γ -ray angular correlations and the data, as shown in Fig 3. The experimental nuclear precession angle, $\Delta\theta_{\text{exp}}$, was extracted from γ -ray count ratios in pairs of detectors at $(\pm\theta, \phi)$ for both field directions, using standard analysis methods as described in [14].

An evaluation of $\Delta\theta/g = (-\mu_N/\hbar) \int B_{\text{tf}} dt$ is required to extract the g factors. Calculations were performed using the code GKINT to take into account the incoming and exiting ion velocities, the energy- and angle-dependent Coulomb excitation cross sections in both target layers, the excited-state lifetimes, and the parametrization of the TF strength in Eq. (1). The results and the g factors extracted are given in Table II. These g factor results are not very sensitive to the somewhat uncertain behavior of the transient field at the highest velocities because (i) the ions spend least time interacting with the TF at high velocity and (ii) the TF strength near $2Zv_0$ is very small. Furthermore, the positive g factor in ^{38}S and

TABLE II: Nuclear parameters and reaction kinematics. $B(E2)\uparrow = B(E2; 0_{\text{gs}}^+ \rightarrow 2_1^+)$. $\langle E_{i,e} \rangle$ and $\langle v_{i,e} \rangle$ are the ion kinetic energies and velocities at the entrance and exit of the iron layer. The effective transient-field interaction time t_{eff} and the spin precession per unit g factor, $(\Delta\theta/g)_{\text{calc}}$, are evaluated for ions that decay after leaving the target. The experimental g factor is given by $g = \Delta\theta_{\text{exp}}/(\Delta\theta/g)_{\text{calc}}$.

Isotope	$E(2_1^+)$ (keV)	$B(E2)\uparrow$ ($e^2\text{fm}^4$)	$\tau(2_1^+)$ (ps)	$\langle E_i \rangle$ (MeV)	$\langle E_e \rangle$ (MeV)	$\langle v_i/Zv_0 \rangle$	$\langle v_e/Zv_0 \rangle$	t_{eff} (ps)	$(\Delta\theta/g)_{\text{calc}}$ (mrad)	$\Delta\theta_{\text{exp}}$ (mrad)	g
^{38}S	1292	235(30)	4.9	762	123	1.75	0.71	2.98	-330	-43(15)	+0.13(5)
^{40}S	904	334(36)	21	782	145	1.73	0.75	2.99	-339	+5(21)	-0.02(6)

the essentially null effect for ^{40}S are both firm observations, independent of the transient-field strength. The experimental uncertainties assigned to the g factors are dominated by the statistical errors in the γ -ray count ratios, with a small contribution (10%) from the angular correlation added in quadrature.

Shell model calculations were performed for $^{36}_{16}\text{S}_{20}$, $^{38}_{16}\text{S}_{22}$ and $^{40}_{16}\text{S}_{24}$, and their isotones $^{38}_{18}\text{Ar}_{20}$, $^{40}_{18}\text{Ar}_{22}$ and $^{42}_{18}\text{Ar}_{24}$, using the code OXBASH [20] and the sd - pf model space where (for $N \geq 20$) valence protons are restricted to the sd shell and valence neutrons are restricted to the pf shell. The Hamiltonian was that developed in Ref. [21] for neutron-rich nuclei around $N = 28$. These calculations reproduce the energies of the low-excitation states to within 200 keV. With standard effective charges of $e_p \sim 1.5$ and $e_n \sim 0.5$ they also reproduce the measured $B(E2)$ values. The g factors of the 2_1^+ states were evaluated using the bare nucleon g factors. The calculated g factors are compared with experimental results in Fig. 4. Overall the level of agreement between theory and experiment is satisfactory given the extreme sensitivity to configuration mixing and the near cancelation of proton and neutron contributions in the $N = 22, 24$ isotones (see below).

In the $N = 20$ isotones, ^{36}S and ^{38}Ar , the 2_1^+ state is a pure proton excitation for our model space. Two neutrons have been added in the fp shell in the $N = 22$ isotones ^{38}S and ^{40}Ar . Since ^{36}S is almost doubly magic, the initial expectation might be that the first-excited state of ^{38}S would be dominated by the neutron $f_{7/2}$ configuration weakly coupled to the ^{36}S core, resulting in a g factor near -0.3 . In contrast, the near zero theoretical g factor and the small but positive experimental g factor require additional proton excitations, which

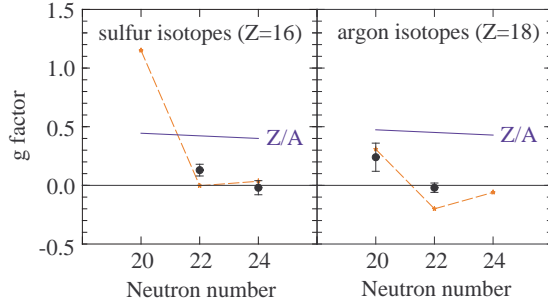


FIG. 4: Theoretical g factors compared with experiment. The previous results for ^{38}Ar and ^{40}Ar are from Refs. [22] and [23], respectively.

indicates strong coupling between protons and neutrons - one of the prerequisites for the onset of deformation. For $N = 22, 24$ the shell model predicts a cancelation of the proton and neutron contributions to the moment; in terms of $g^{\text{th}} = g_{\text{proton}}^{\text{th}} + g_{\text{neutron}}^{\text{th}}$, $g(^{38}\text{S}) = -0.003 = 0.298 - 0.301$, $g(^{40}\text{S}) = 0.035 = 0.276 - 0.241$, $g(^{40}\text{Ar}) = -0.200 = 0.164 - 0.364$ and $g(^{42}\text{Ar}) = -0.060 = 0.220 - 0.280$. The proton contributions to the g factors are dominated by the orbital component but the substantial neutron contributions originate entirely with the intrinsic spin associated with a dominant occupation of the neutron $f_{7/2}$ orbit. Some tuning of the Hamiltonian may be required to reproduce the sign of the g factor in ^{38}S , which is very sensitive to the separation of the proton $s_{1/2}$ and $d_{3/2}$ orbitals, for example. The dependence of the $g(2^+)$ in ^{40}Ar on the basis space, the interaction, and the choice of effective nucleon g factors, has been investigated in Ref. [23].

As noted above, Coulomb-excitation studies and the level scheme of ^{40}S suggest that it is deformed. Supporting this interpretation, the shell model calculations predict consistent intrinsic quadrupole moments when derived from either the $B(E2)$ or the quadrupole moment, $Q(2_1^+)$, implying a prolate deformation of $\beta \approx +0.3$, in agreement with the value deduced from the experimental $B(E2)$ [3, 24]. But the near zero magnetic moment does not conform to the usual collective model expectation of $g \sim Z/A$. Since the shell model calculations reproduce both the electric and magnetic properties of the 2_1^+ state they give insight into the reasons for this unprecedented magnetic behavior in an apparently deformed nucleus. The essential difference between the deformed neutron-rich sulfur isotopes and the deformed nuclei previously encountered (i.e. either light nuclei with $N = Z$ or heavier deformed nuclei) is that the spin contributions to the magnetic moments are relatively more

important, especially for the neutrons. In comparison to ^{40}S , the 2_1^+ state in the $N = 20$ nucleus $^{32}_{12}\text{Mg}_{20}$ has a similar excitation energy, lifetime and $B(E2)$. However the g factor in ^{32}Mg might be closer to that of a conventional collective nucleus since the $N = 20$ shell closure is known to vanish far from stability.

We thank the NSCL operations staff for providing the primary and secondary beams for the experiment. This work was supported by NSF grants PHY-01-10253, PHY-99-83810, and PHY-02-44453. AES, ANW, and PMD acknowledge travel support from the ANSTO AMRF scheme (Australia).

-
- [1] S. Grévy, *et al.*, Phys. Lett. B **594**, 252 (2004).
 - [2] J. Fridmann, *et al.*, Nature **435**, 922 (2005).
 - [3] H. Scheit, *et al.*, Phys. Rev. Lett. **77**, 3967 (1996).
 - [4] T. Glasmacher, *et al.*, Phys. Lett. B **395**, 163 (1997).
 - [5] J. Winger, P. Mantica, R. Ronningen, and M. Caprio, Phys. Rev. C **64**, 064318 (2001).
 - [6] D. Sohler, *et al.*, Phys. Rev. C **66**, 054302 (2002).
 - [7] P. D. Cottle and K. W. Kemper, Phys. Rev. C **58**, 3761 (1998).
 - [8] R. Rodríguez-Guzmán, J. Edigo, and L. Robledo, Phys. Rev. C **65**, 024304 (2002).
 - [9] E. Caurier, F. Nowacki, and A. Poves, Nucl. Phys. A **742**, 14 (2004).
 - [10] A. E. Stuchbery, Phys. Rev. C **69**, 064311 (2004).
 - [11] T. Glasmacher, Annu. Rev. Nucl. Sci. **48**, 1 (1998).
 - [12] N. Benczer-Koller, M. Hass, and J. Sak, Annu. Rev. Nucl. Sci. **30**, 53 (1980).
 - [13] K. H. Speidel, O. Kenn, and F. Nowacki, Prog. Part. Nucl. Phys. **49**, 91 (2002).
 - [14] A. E. Stuchbery, *et al.*, Phys. Lett. B **611**, 81 (2005).
 - [15] D. J. Morrissey, *et al.*, Nucl. Inst. Meth. Phys. Res. B **204**, 90 (2003).
 - [16] W. F. Mueller, *et al.*, Nucl. Inst. Meth. Phys. Res. A **466**, 492 (2001).
 - [17] A. E. Stuchbery, *Some notes on the program GKINT: Transient-field g-factor kinematics at intermediate energies*, Department of Nuclear Physics, The Australian National University, report no. ANU-P/1678 (2005).
 - [18] C. A. Bertulani, A. E. Stuchbery, T. J. Mertzimekis, and A. D. Davies, Phys. Rev. C **68**, 044609 (2003).

- [19] A. E. Stuchbery, P. M. Davidson, and A. N. Wilson, Nucl. Instr. Meth. Phys. Res. B **243**, 265 (2006).
- [20] B. A. Brown, *et al.*, *Oxbash for Windows PC*, Michigan State University, report no. MSU-NSCL 1289 (2004).
- [21] S. Nummela, *et al.*, Phys. Rev. C **63**, 044316 (2001).
- [22] K.-H. Speidel, *et al.*, Phys. Lett. B **632**, 207 (2006).
- [23] E. Stefanova, *et al.*, Phys. Rev. C **72**, 014309 (2005).
- [24] J. Retamosa, E. Caurier, F. Nowacki, and A. Poves, Phys. Rev. C **55**, 1266 (1997).